BIOLOGY OF REPRODUCTION (2015) **92**(3):67, 1–18
Published online before print 7 January 2015.
DOI 10.1095/biolreprod.114.125708

Identifying a Novel Role for X-prolyl Aminopeptidase (*Xpnpep*) 2 in CrVI-Induced Adverse Effects on Germ Cell Nest Breakdown and Follicle Development in Rats[1]

Sakhila K. Banu,[2] Jone A. Stanley, Kirthiram K. Sivakumar, Joe A. Arosh, Rola Barhoumi, and Robert C. Burghardt

Department of Veterinary Integrative Biosciences, College of Veterinary Medicine and Biomedical Sciences, Texas A&M University, College Station, Texas

ABSTRACT

Environmental exposure to endocrine-disrupting chemicals (EDCs) is one cause of premature ovarian failure (POF). Hexavalent chromium (CrVI) is a heavy metal EDC widely used in more than 50 industries, including chrome plating, welding, wood processing, and tanneries. Recent data from U.S. Environmental Protection Agency indicate increased levels of Cr in drinking water from several American cities, which potentially predispose residents to various health problems. Recently, we demonstrated that gestational exposure to CrVI caused POF in F1 offspring. The current study was performed to identify the molecular mechanism behind CrVI-induced POF. Pregnant rats were treated with 25 ppm of potassium dichromate from Gestational Day (GD) 9.5 to GD 14.5 through drinking water, and the fetuses were exposed to CrVI through transplacental transfer. Ovaries were removed from the fetuses or pups on Embryonic Day (ED) 15.5, ED 17.5, Postnatal Day (PND) 1, PND 4, or PND 25, and various analyses were performed. Results showed that gestational exposure to CrVI: 1) increased germ cell/oocyte apoptosis and advanced germ cell nest (GCN) breakdown; 2) increased X-prolyl aminopeptidase (Xpnpep) 2, a POF marker in humans, during GCN breakdown; 3) decreased Xpnpep2 during postnatal follicle development; and 4) increased colocalization of Xpnpep2 with Col3 and Col4. We also found that Xpnpep2 inversely regulated the expression of Col1, Col3, and Col4 in all the developmental stages studied. Thus, CrVI advanced GCN breakdown and increased follicle atresia in F1 female progeny by targeting Xpnpep2.

chromium, collagen, follicle atresia, follicle maturation, germ cell nest breakdown, oocyte, ovary, premature ovarian failure, primordial follicle, Xpnpep2

INTRODUCTION

Premature ovarian failure (POF) is a defect of ovarian follicle development and is characterized by primary or secondary amenorrhea, with elevated levels of serum gonadotropins, or by early menopause [1, 2]. The disorder has been attributed to various causes, including exposure to endocrine-disrupting chemicals (EDCs). Our recent report showed that gestational exposure to hexavalent chromium (CrVI) caused POF in first-generation (F1) female offspring [3]. POF affects approximately 1 in 10 000 women by the age of 20 yr, 1 in 1000 women by 30 yr, and 1 in 100 women by 40 yr [4]. In approximately 30% of patients with POF, this condition is caused by defined genetic alterations, including mutations in *FoxL2*, deletions within the X-chromosome, and fragile X chromosome mutations [5, 6]. Identification of the etiological basis for POF in the remaining 70% of patients is a pressing clinical need because relatively few treatment options have been developed for these women [7]. Exposure to EDCs leads to a reduced initial primordial follicle pool [8, 9] and/or an accelerated decline in primordial follicle number [10, 11]. This will ultimately decrease the reproductive life span of affected females by reducing the primordial follicle pool below the critical threshold necessary to maintain ovarian activity.

Primordial follicles form during gestation in humans but after birth in rodents in a process that involves dissolution of germ cell syncytia, or germ cell nests (GCNs), that form during germ cell mitosis [12]. The process of GCN breakdown involves migration of somatic/pregranulosa cells into the GCN and simultaneous disruption of the interoocyte bridges through apoptosis of individual oocytes [13]. The pregranulosa cells then surround the remaining oocytes to form primordial follicles that constitute the resting stock of gametes for the entire reproductive life span of mammalian females [12]. Thus, any alteration in this process might lead to a reduced primordial follicle pool size, resulting in POF.

Cytogenetic and molecular analyses of women with POF carrying a balanced X-autosome translocation allowed the identification of a ''critical region'' for ovarian development and function on the long arm of the X chromosome from Xq13.3 to Xq27. This region could be split into two functionally different portions: Xq13–21 and Xq23–27 [14, 15]. Breakpoints in the Xq13–21 region are responsible for balanced translocations, whereas breakpoints in the Xq23–27 region result in interstitial deletions. Heterochromatin rearrangements of the Xq13–21 region were reported to downregulate oocyte-expressed genes during oocyte and follicle maturation, indicating that X-linked POF may be an epigenetic disorder [16]. Translocations that affect X chromosome structure increase apoptosis of germ cells [17], leading to POF. Direct disruption of relevant loci or a ''position effect'' caused by the rearrangements on contiguous genes can also result in POF. Transcriptional characterization of breakpoint regions in balanced translocations led to the identification of five genes interrupted by translocations (the *Xpnpep2* gene in Xq25 [18], the *POF1B* gene in Xq21.2 [19], the *DACH2* gene in Xq21.3 [19], the *CHM* gene in Xq21.2 [20], and the

[1]Supported by National Institute of Environmental Health Sciences grant ES020561-01 (to S.K.B.), Center for Translational Environmental Health Research grant P30ES023512 (to S.K.B, R.C.B, R.B), and National Institutes of Health National Center for Research Resources Shared Instrumentation Grant 1 S10 RR22532-01 (to R.C.B.).
[2]Correspondence: Sakhila K. Banu, Department of Integrative Biosciences, College of Veterinary Medicine and Biomedical Sciences, Texas A&M University, College Station, Texas 77843.
E-mail: skbanu@cvm.tamu.edu

Received: 9 October 2014.
First decision: 23 November 2014.
Accepted: 30 December 2014.

eISSN: 1529-7268 http://www.biolreprod.org
ISSN: 0006-3363

DIAPH2 gene in Xq22 [21]) and classified as POF marker genes in humans. However, the mechanism by which translocations in the Xq critical region may cause POF is not clear. Prueitt et al. [18, 22] mapped POF-associated breakpoints, including *Xpnpep2*. However, the role of *Xpnpep2* in female fertility is currently unknown.

The *Xpnpep2* gene encodes the protein X-propyl aminopeptidase, which belongs to the family of ''pita bread'' metalloenzymes. It is expressed in prokaryotes and eukaryotes and hydrolyzes N-terminal Xaa-Pro bonds, where proline is the penultimate residue. Mammals have both a membrane-bound and a soluble Xpnpep2, with different tissue distributions [23]. The membrane-bound Xpnpep2 is a heavily glycosylated glycosylphosphatidylinositol-anchored protein of 673 amino acids encoded by the *Xpnpep2* gene on human Xq25 [24]. Several biologically active polypeptides, including collagens (Cols), hormones, growth factors, and cytokines, contain N-terminal Xaa-Pro sequences and therefore are potential substrates for *Xpnpep2*. Because Cols contain a high proportion of such ''triplets,'' *Xpnpep2* has the potential for intracellular (lysosomal) degradation of Col fibrils [25–27]. In fact, proline and hydroxyproline constitute 20%–25% of the residues in Cols [26], and none of the lysosomal proteinases is capable of cleaving these linkages [27].

Within the ovary and follicle, the extracellular matrix (ECM), including Cols, provides structural support, organizes and connects cells, serves as a reservoir for signaling molecules and growth factors that regulate follicle growth, provides a filtration barrier, and guides cell migration [28, 29]. The ECM also regulates establishment of the basement membrane, oocyte maturation, follicle atresia, steroidogenesis, and cell lineage [29–32]. The ECM components of the basal membrane affect follicle development in the ovary and are important for maintaining the polarity and the degree of polarization of granulosa cells [33–35]. A recent study found that Col1 is spatially and temporally expressed in immature rat ovaries and is regulated by gonadotropins, suggesting a role for Col1 in morphogenesis of follicles as well as corpus luteum formation and regression [36]. Col1 is expressed in the basal lamina of follicles and participates in the organization of the basal lamina [37]. Another study using *Esr2*-null mice showed that *Esr2* regulates *Col* gene expression in the ovary before puberty. Dysregulation of *Esr2*-mediated ECM gene expression in early postnatal life disrupts folliculogenesis and contributes to the impaired response of immature *Esr2*-null granulosa cells to follicle-stimulating hormone [38].

Hexavalent chromium has been used in various industries, such as leather and textiles, metallurgical, chemical, and automotive [39]. Due to increased use and improper disposal of CrVI, its levels in the water, soil, and air continue to increase [40, 41]. Significant contamination with CrVI has been found in the drinking water sources of more than 30 U.S. cities [42]. Women working in dichromate manufacturing industries and tanneries and living around Cr-contaminated areas have high levels of Cr in blood and urine and encounter gynecological illness, abortion, postnatal hemorrhage, and birth complications [43–46]. Welding fumes and metal dusts containing CrVI are known to be either teratogenic, carcinogenic, embryotoxic, or mutagenic [47]. Previous epidemiological studies have found an increased risk of spontaneous abortion among women employed by metal industries in Finland [48, 49] and chromate factories in China [50]. The presence of Cr in umbilical cord blood and placental tissue in these women directly correlates with an increased risk of abortion [48, 49]. In addition, occupational exposure to CrVI during pregnancy also decreased intrauterine growth of fetuses, resulting in low birth weight [50]. Exposure to heavy metals during pregnancy increases oxidative stress in the maternal and fetal compartments [51], resulting in adverse pregnancy outcomes. However, while Cr is known to adversely affect reproductive health in women [48, 49], the specific mechanisms of reproductive toxicity are not clearly understood.

Hexavalent chromium enhances oxidative stress in vivo and in vitro [52–54]. The reduction of CrVI into CrV induces DNA damage and mutations [55]. Genotoxic effects of Cr are predominantly represented by the formation of oxidative adducts and apurinic/apyrimidinic lesions, eventually resulting in DNA breaks [56–58]. Cr also exhibits epigenetic effects [59]. CrVI causes oxidative DNA damage and increases 8-oxo-7,8-dihydroguanine (8-oxoG) [60]. Kim et al. [61] demonstrated increased 8-oxoG in the aging mouse ovary. The increase of 8-oxoG in DNA results in a GC-to-TA transversion during DNA replication [62–65]. Strikingly, many data demonstrate the role of CrVI in epigenetic modifications [59, 66–68]. Examples include decreased histone acetylation in human branchial epithelial cells [69] as well as increased DNA methylation in the promoter region of the DNA mismatch repair (*MLH1*) gene [70] and *CDKN2A (P16)* [71] in human lung cancers. Thus, CrVI exhibits both genotoxic effects and epigenetic modifications in human cancers. Interestingly, such mechanisms have not been reported in the ovary. Identifying such mechanisms can potentially help to fill the gap in knowledge regarding the role of CrVI in causing POF. Therefore, the main goal of the current investigation was to determine the effect of prenatal exposure to CrVI on the spatiotemporal expression pattern of Xpnpep2 and its substrates, Col1, Col3, and Col4, during fetal and postnatal development of the ovary.

MATERIALS AND METHODS

In Vivo Dosing of Animals and Experimental Design

Pregnant Sprague Dawley rats (age, 60–70 days) were divided into two groups: control (n = 25) and CrVI (n = 25). Control rats received regular drinking water and diet ad libitum. Rats from the CrVI group received 25 ppm of potassium dichromate in drinking water from Gestational Day (GD) 9.5 to GD 14.5. The first and second sets of control (n = 5 per set) and CrVI (n = 5 per set) rats were euthanized on GD 15.5 and GD 17.5, respectively. The third and fourth sets of control (n = 5 per set) and CrVI (n = 5 per set) rats were allowed to deliver pups (F1 pups). Ovaries from F1 pups were removed on Postnatal Day (PND) 1 and PND 4 for further analyses. The fifth set of F1 pups from control (n = 5) and CrVI (n = 5) rats were maintained in a separate cage with their respective mothers, weaned on PND 22, fed with regular drinking water and diet ad libitum, and euthanized on PND 25. Blood and the ovaries were collected from these pups for further analyses. Animal use protocols were approved by the Animal Care and Use Committee of Texas A&M University and were in accordance with the standards established by Guiding Principles in the Use of Animals in Toxicology and Guidelines for the Care and Use of Experimental Animals by National Institute of Health.

Histology

Histological processing of the ovary was performed by the Histology core lab facility, College of Veterinary Medicine & Biomedical Sciences, Texas A&M University, based on the standard protocols for paraffin-embedded sections that were cut at a thickness of 5 μm and stained with hematoxylin-and-eosin (H&E).

TUNEL Assay

Paraffin-embedded tissue sections were deparaffinized and TUNEL assay performed as described elsewhere [3, 52, 53]. The apoptosis index was calculated as the average percentage of TUNEL-positive germ cells/oocytes from 20 ovaries at 400× magnification. To avoid choosing the same follicle or oocyte, we used every 12th unstained section of the ovary from PND 1 and PND 4 and every 40th unstained section of the ovary from PND 25 as described

by Devine et al. [72]. Only oocyte-containing follicles were counted. For Embryonic Day (ED) 15.5 and ED 17.5, we used every 10th section. We employed this method to analyze ovarian sections for TUNEL, H&E, and immunohistochemistry (IHC) to avoid repeating the measurements on the same oocyte/follicle. Germ cells/oocytes from 20 to 35 fields were counted for ED 15.5, ED 17.5, PND 1, and PND 4, and those from 200 fields were counted for PND 25.

Immunohistochemistry

Sources of antibodies, catalog numbers, dilutions, host species, immunogens, and homologies with rat/mouse are given in Table 1. Ovaries were fixed in 4% buffered paraformaldehyde for 1 h at 4°C and processed using standard procedures as described elsewhere [3, 52]. The tissue sections were incubated with primary antibodies for Embp, Xpnpep2, Col1, Col3, and Col4 at specific concentrations (Table 1). To determine the abundance of each protein, we included both healthy follicles and atretic follicles from the CrVI-exposed ovaries using blind and random selection criteria. Digital images were captured using a Zeiss Axioplan 2 Research Microscope (Carl Zeiss) with an Axiocam HR digital color camera. The intensity of staining for each protein was quantified using Image-ProPlus 6.3 image processing and analysis software according to the manufacturer's instructions (Media Cybernetics, Inc.). In brief, six images of the ovary at 400× magnification were captured randomly without hot-spot bias in each tissue section per animal. Integrated optical density of immunostaining was quantified in the RGB mode. Numerical data were expressed as the least square mean ± SEM. This technique is more quantitative than conventional blind scoring systems, and the validity of the quantification was reported previously by our group [73].

Analysis of Oocyte Numbers

Oocyte numbers were determined by counting the number of germ cells positive for the germ cell marker, Vasa, found within each optical section used for analyzing GCN breakdown and follicle development. The numbers were averaged and reported as number of oocytes per ovary in percentage.

Whole-Mount Double Immunofluorescence Staining

Whole-mount double immunofluorescence staining was performed as described previously [3, 74]. In brief, the ovaries were fixed with 5.3% formaldehyde (catalog no. 18814; Polysciences) overnight at 4°C. After several washings with PBS, they were labeled with primary antibodies overnight at 4°C for both Vasa and the somatic cell marker, Gata4; Xpnpep2 and Col3; or Xpnpep2 and Col4 at the appropriate dilution (Table 1). The ovaries were incubated with fluorophore-conjugated secondary antibodies for 4 h at room temperature and overlaid with a cover glass and mounting medium containing Prolong Gold Antifade Reagent (Life Technologies). Images were obtained on a Zeiss LSM 510 confocal microscope with a plan apochromat 63×/1.4 NA oil objective. For the green dye, an argon laser set was used with an excitation of 488 nm and emission (collected with a band-pass filter) of 500–550 nm. For the red dye, a helium-neon laser was used with an excitation of 543 nm and emission (collected with a long-pass filter) of 560 nm. At least eight images were collected per treatment.

Analysis of GNC Breakdown and Follicle Development

For each ovary, two cores were visualized and counted. A core is a region 135 × 135 μm consisting of optical sections at four different depths in the ovary, each 15–20 μm apart. Thus, for each ovary, two cores were obtained consisting of four optical sections per core for a total of eight optical sections per ovary. The number of germ cells found in the cyst relative to the total number of oocytes was determined for each ovary by analyzing each section and was reported as the percentage of single oocytes. To determine whether oocytes were in cysts, a Z-stack of images, each 1 μm apart, for each of the four optical sections in a core was obtained, with five images above the section and five images below the section being analyzed. This allowed us to determine whether an oocyte was part of a GCN above or below the plane of focus [3, 74].

Statistical Analysis

Effects of CrVI on various parameters in the ovary were analyzed and the results expressed as the mean ± SEM. Student *t*-test was used to compare groups, and *P*-values of less than 0.05 were considered to be statistically significant.

TABLE 1. Sources of antibodies, catalog numbers, dilutions, host species, immunogens, and homologies with rat/mouse.

Antibody	Company (catalog no.)	Dilution	Host species	Immunogen	Percentage homology with rat/mouse	Secondary antibody	Dilution	Application
Col1	Abcam (AB292)	1:500	Rabbit polyclonal	Human	Rat: 91%; mouse: 92%	Goat anti-rabbit	1:200	IHC
Col3	Sigma (C7805)	1:100	Mouse monoclonal	Human	Rat: 94%; mouse: 94%	Horse anti-mouse	1:200	IHC
Col4	Sigma (SAB4200500)	1:750	Mouse monoclonal	Human	Rat: 89%; mouse: 94%	Horse anti-mouse	1:200	IHC
Xpnpep2	Abcam (AB97852)	1:100	Rabbit polyclonal	Human	Rat: 84%; mouse: 86%	Goat anti-rabbit	1:200	IHC
Embp	Santa Cruz (SC-33938)	1:250	Goat polyclonal	Mouse	Rat: 87%; mouse: 100%	Rabbit anti-goat	1:100	IHC
Gata4	Santa Cruz (SC-1237)	1:50	Goat polyclonal	Mouse	Rat: 100%; mouse: 100%	Goat anti-mouse Alexa 594 red	1:200	Immuno-colocalization
Vasa	Abcam (AB13840)	1:100	Rabbit polyclonal	Human	Rat: 95%; mouse: 98%	Goat anti-mouse Alexa 488 green	1:200	Immuno-colocalization

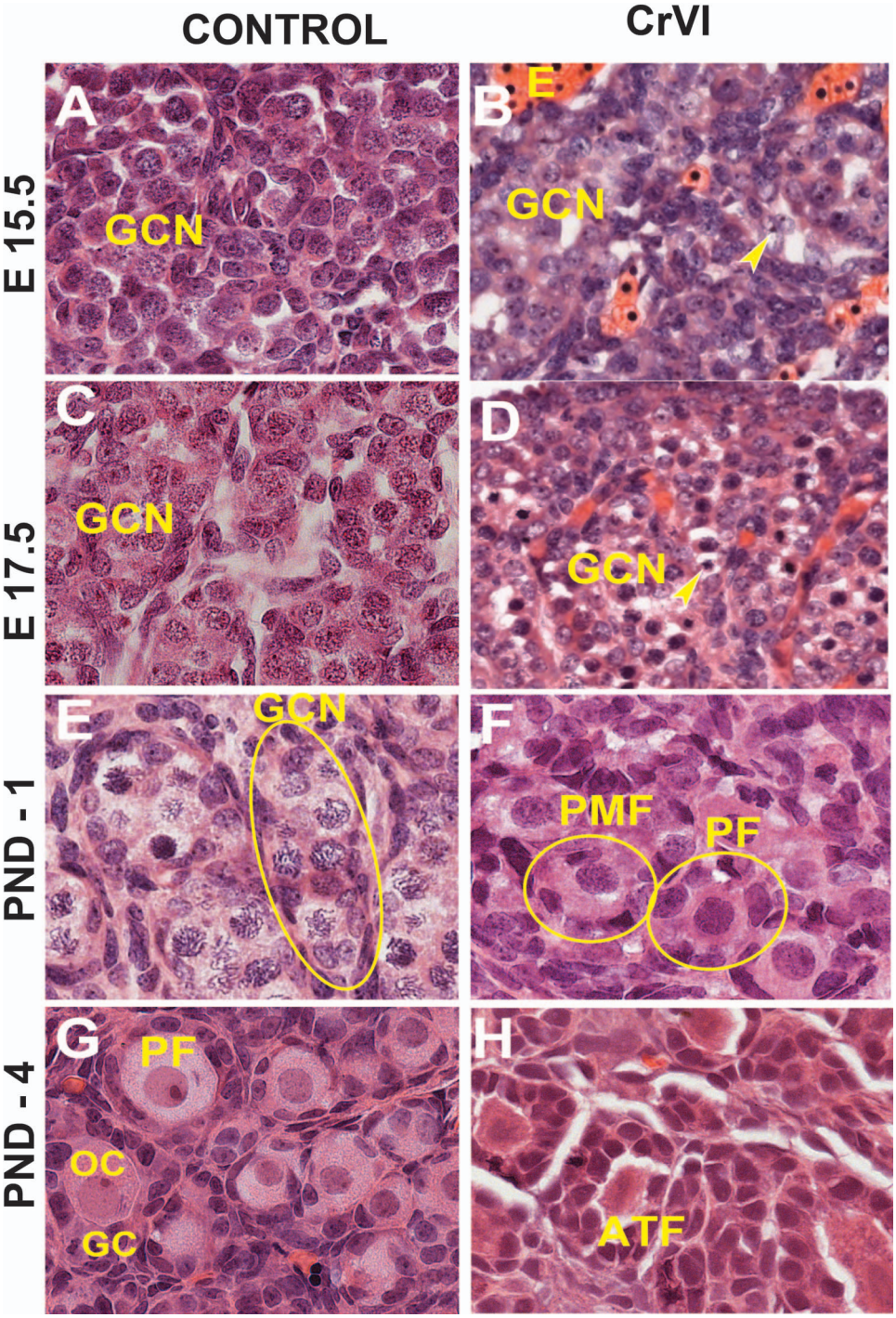

FIG. 1. Effects of prenatal exposure to CrVI on germ cell degradation and eosinophilic infiltration in the ovary. Pregnant mother rats (F0; n = 5) received either regular drinking water (control) or CrVI (potassium dichromate, 25 ppm; n = 10) in drinking water from GD 9.5 to GD 14.5. During this period, fetuses were exposed to CrVI via transplacental transfer. On ED 15.5 and ED 17.5, ovaries from the fetuses were removed. On PND 1 and PND 4, ovaries were removed from F1 female pups and processed for histology (H&E). The width of field for each image is 220 or 350 μm. Arrowheads indicate pyknotic nuclei. Representative images are shown for ED 15.5 (**A** and **B**), ED 17.5 (**C** and **D**), PND 1 (**E** and **F**), and PND 4 (**G** and **H**). E, eosinophils; PMF, primordial follicle; PF, primary follicle; ATF, atretic follicle; OC-oocyte; GC, granulosa cells.

RESULTS

Effects of CrVI on Germ Cell Viability, Follicle Development, and Follicle Atresia

On ED 15.5 and ED 17.5, control ovaries were packed with rounded GCN containing healthy germ cells and few degenerating germ cells. In contrast, greater numbers of degenerating germ cells with pyknotic nuclei were observed in CrVI animals on ED 15.5 and ED 17.5 (Fig. 1, A–D). On PND 1, control ovaries were filled with nests of healthy germ cells surrounded by invading somatic or pregranulosa cells, whereas CrVI treatment accelerated GCN breakdown and advanced primordial and primary follicle formation (Fig. 1, E and F). On PND 4, control ovaries were predominantly filled

with healthy primordial and few primary follicles, whereas ovaries from the CrVI rats had several primary and few secondary follicles. Interestingly, CrVI decreased healthy primordial and primary follicles and increased follicle atresia in rats exposed to CrVI in utero (Figs. 1, G and H, and 2).

Germ cell death is one of the major events that occur during GCN breakdown and follicle formation. Approximately one-third of the primordial follicles undergo atresia within a few days after birth [75]. In the current study, CrVI increased the number of TUNEL-positive germ cells on ED 15.5, ED 17.5, PND 1, PND 4, and PND 25 compared to control (Fig. 2) and increased eosinophilic infiltration on ED 15.5 and ED 17.5 (Fig. 3). CrVI increased germ cell death. Several pyknotic nuclei were found within the GCN.

Effects of CrVI on GCN Breakdown

Effects of CrVI on GCN breakdown were determined by coimmunolocalization of the germ cell marker, Vasa, and the somatic cell marker, Gata4, in whole-mount ovaries. Control ovaries at ED 15.5 and ED 17.5 consisted of clusters of 10–29 intact and healthy germ cells within a GCN with no primordial follicles (Figs. 4 and 5). In CrVI rats, GCNs were broken down into smaller nests on ED 15.5 and ED 17.5 (Figs. 4 and 5). In particular, penetration of the somatic cells in between the germ cells was very obvious on ED 15.5 and ED 17.5 in CrVI-exposed ovaries compared to control ovaries.

Spatiotemporal Expression of Xpnpep2 and Its Relationship to Col1, Col3, and Col4 Distribution During GCN Breakdown and Follicle Development

The *Xpnpep2* gene is one of the marker genes for POF in women [18, 22] and is involved in the hydrolysis of Cols [27]. We recently showed that gestational exposure to CrVI induced POF in F1 rats [3]. To understand the role of Xpnpep2 in regulating the distribution of Cols during GCN breakdown and ovarian development, we determined the distribution of Xpnpep2, Col1, Col3, and Col4 in the ovaries on ED 15.5, ED 17.5, PND 1, PND 4, and PND 25.

On ED 15.5, the expression of Xpnpep2 was greater in the ovaries of CrVI-treated animals compared to control (Fig. 6, A–C). In the control ovaries, Col1 was highly expressed, with the Col1 bundles thicker along the ovigerous cords surrounding the GCN, and minimally expressed inside the GCN and between the germ cells (Fig. 6, D–F). CrVI significantly decreased the expression of Col1, and because the GCN had broken down to smaller nests, the penetration of Col1 within the nests and a few single oocytes was very obvious. In control ovaries on ED 15.5, Col3 and Col4 were distributed along the ovigerous cords (borders surrounding the GCN). CrVI down-regulated the expression of Col1, Col3, and Col4 (Fig. 6, D–L).

On ED 17.5, ovaries from both control and CrVI groups had high expression of Xpnpep2, although expression was significantly greater in the CrVI group (Fig. 7, A–C). Col1 was expressed in both control and CrVI groups, whereas Col1 was significantly decreased in the CrVI group (Fig. 7, D–F). In the control group, Col1 was distributed at the periphery of the GCN along the ovigerous cords. In the CrVI group, Col1 was distributed around the smaller and disrupted nests of germ cells, with an increased thickness of Col bundles. Col3 and Col4 expression was very low, being sporadic and homogeneous in both control and CrVI-exposed ovaries, with a slight increase in ovarian surface epithelium (OSE) in the control ovaries.

On PND 1, CrVI significantly decreased ovarian Xpnpep2 levels compared to control (Fig. 8, A–C). Xpnpep2 was localized primarily within the oocytes compared to surrounding stroma and/or somatic cells. Accompanying the decreased Xpnpep2 levels in CrVI-treated animals, the expression of Col1, Col3, and Col4 was significantly increased compared to control animals (Fig. 8, D–L). The elevated Col1, Col3, and Col4 levels were predominantly localized around follicular basal lamina (Fig. 8, E, H, and K).

On PND 4, Xpnpep2 was highly expressed in the oocytes and moderately expressed in granulosa cells of control ovaries. In the CrVI group, Xpnpep2 was expressed only in the oocytes and at a very low level (Fig. 9, A–C), and the expression of Col1, Col3, and Col4 was elevated compared to control. Col1, Col3, and Col4 were distributed in the follicular basal lamina, stroma, and interstitium in both the control and CrVI groups (Fig. 9, D–L).

On PND 25, Xpnpep2 remained highly expressed in the oocytes and granulosa cells of control ovaries and barely detectable in CrVI-exposed ovaries (Fig. 10, A–C). In the control ovaries, Col1 was highly expressed in the follicular basal lamina, stroma, and theca/interstitial cells and in the OSE (Fig. 10D). In the CrVI-treated animals, Col1 expression was elevated in the granulosa cells, follicular fluid, follicular basal lamina, stroma, and interstitium (Fig. 10E). In both the control and CrVI groups, Col3 and Col4 were expressed around the oocytes, within the granulosa cells, and around the antrum and follicular basal membrane (Fig. 10, G–L); however, CrVI up-regulated Col3 and Col4 and increased their expression within the oocyte, follicular fluid, follicular basal lamina, and theca interstitium (Fig. 10, H and K).

Xpnpep2 Is Colocalized with Col3 and Col4 in Fetal Ovaries

Data from the IHC showed a significant negative correlation between the expressions of Xpnpep2 and Col1, Col3, and Col4. To confirm the colocalization of Xpnpep2 and Cols, we performed whole-mount double immunofluorescence labeling of Xpnpep2 with Col3 and Col4 on ED 17.5. Xpnpep2 was colocalized with Col3 (Fig. 11, A–F) and Col4 (Fig. 12, A–F) in both control and CrVI groups around the germ cells, GCN, and along the ovigerous cords. However, CrVI significantly increased colocalization of Xpnpep2 with Col3 (Fig. 11G) and Col4 (Fig. 12G).

DISCUSSION

Germ cell nest breakdown is a prerequisite for the development of primordial follicles [12]. Defects in either the timing or the process of GCN breakdown can result in improper primordial follicle assembly and/or accelerated atresia, resulting in POF or infertility. In most mammals, primordial follicles form either before or during the first few days after birth [76–78]. One-third of the primordial follicles undergo rapid atresia within a few days after birth. The number of primordial follicles that ultimately survive determines the lifetime follicle reserve [79]. Data indicate that CrVI induces germ cell death in the ovary and increased eosinophilic infiltration. Secretory proteins of eosinophils, such as the major basic and cationic proteins, can disrupt cellular membranes and cause degradation of messenger RNA [80]. Eosinophil peroxidase has been shown to augment the ability of macrophages to phagocytize tumor cells [81]. We suggested that increased eosinophils in CrVI-exposed ovaries may

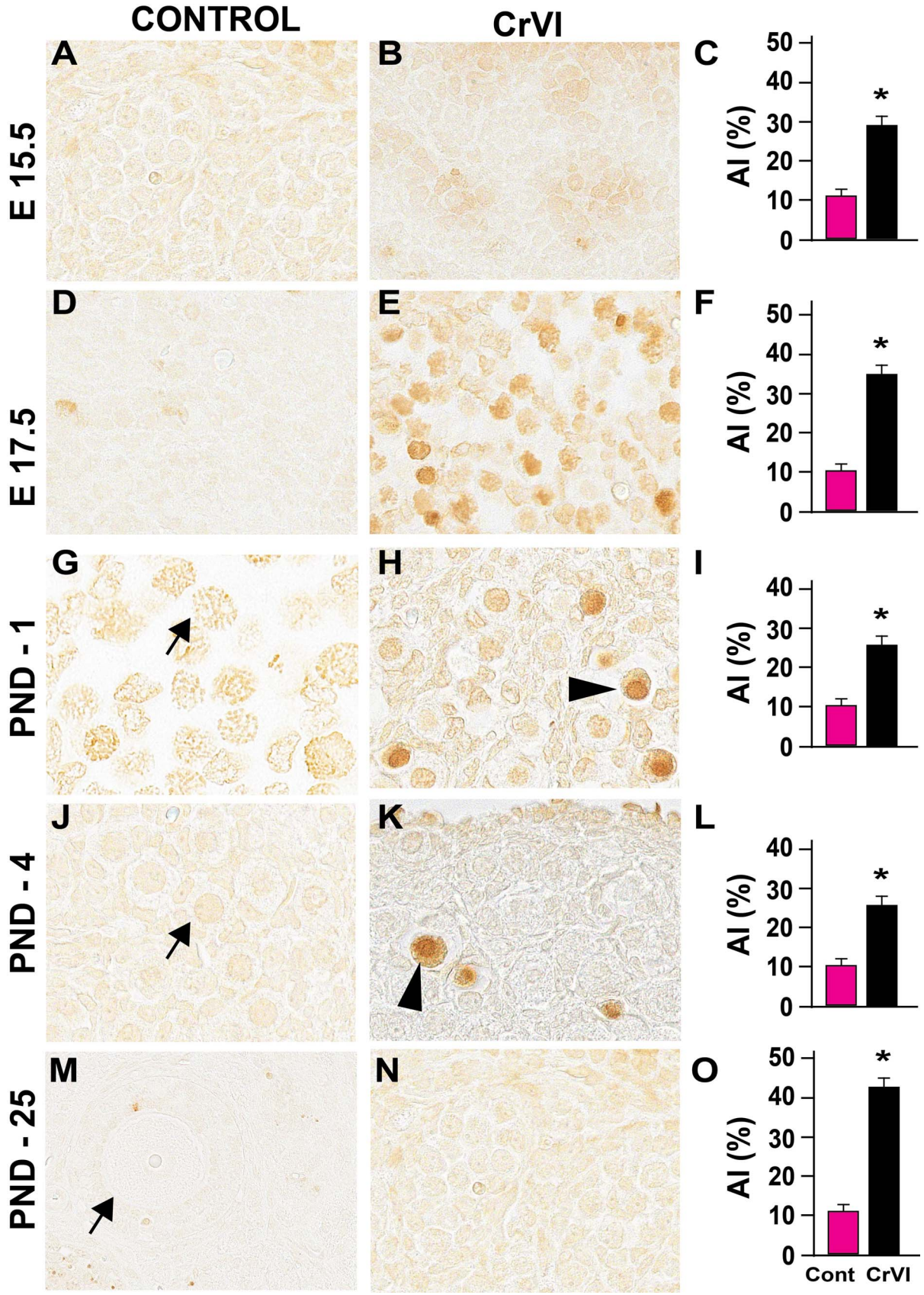

FIG. 2. Effects of prenatal exposure to CrVI on germ cell/oocyte apoptosis. The apoptosis index (AI) was calculated as the average percentage of TUNEL-positive germ cells/oocytes from 20 ovaries. Average number of TUNEL-positive cells in each control group was considered to be 10%. Each value represents the mean ± SEM of TUNEL-positive germ cells/oocytes counted from 25 fields at ED 15.5 (**A**–**C**); from 30 to 35 fields at ED 17.5 (**D**–**F**), PND 1 (**G**–**I**), and PND 4 (**J**–**L**), and 195 fields in PND 25 (**M**–**O**). The width of field for each image is 220 or 350 μm. Arrowheads indicate TUNEL-positive (apoptotic) germ cells or oocytes; arrows indicate healthy germ cells or oocytes. *$P < 0.05$, control vs. CrVI.

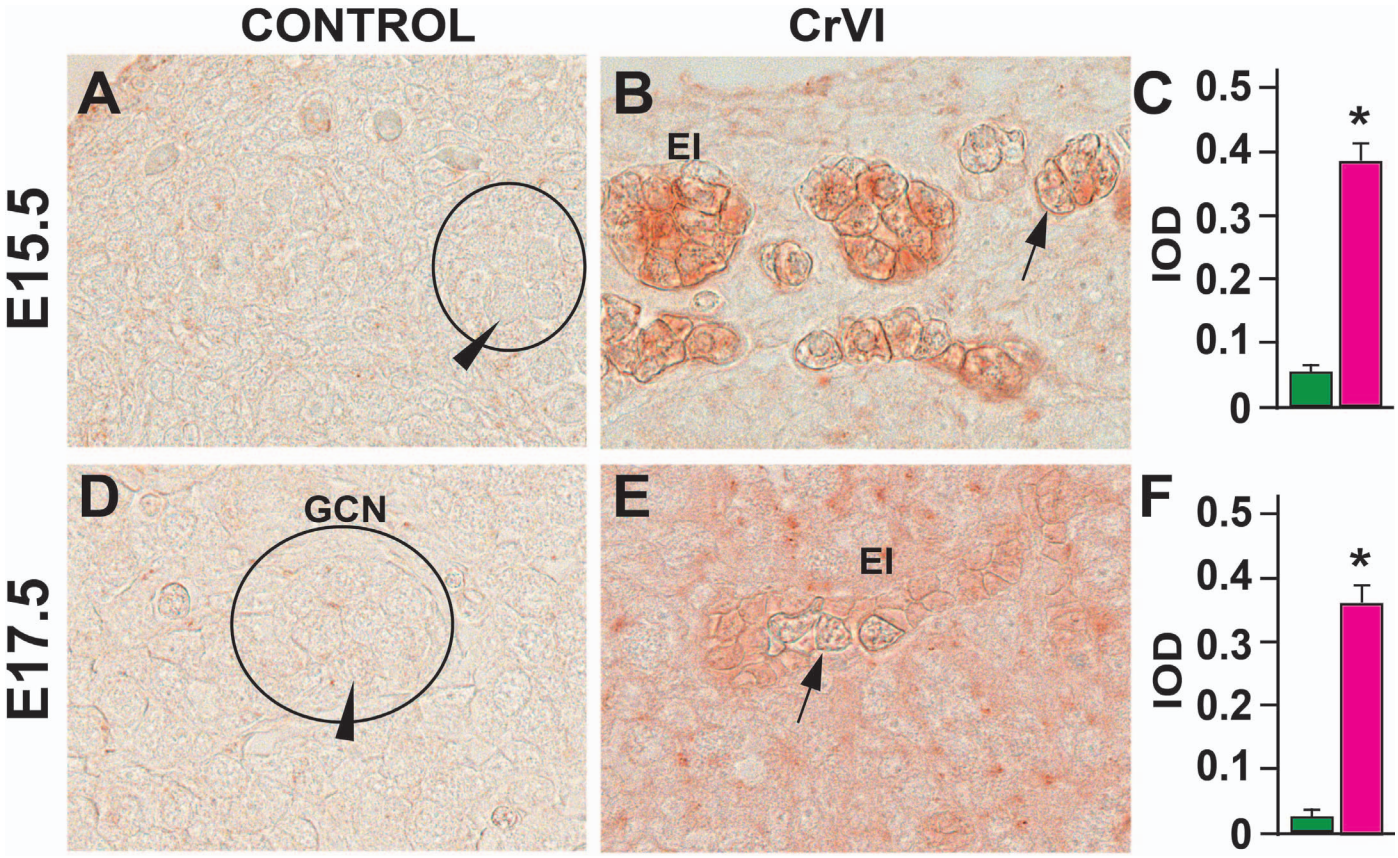

FIG. 3. Effects of prenatal exposure to CrVI on expression of eosinophilic major basic protein (EMBP) in the ED 15.5 (**A**–**C**) and ED 17.5 (**D**–**F**) ovaries. On ED 15.5 and ED 17.5, ovaries from fetuses were removed and processed for IHC. Integrated optical density (IOD) was quantified by Image ProPlus software. Each value represents the mean ± SEM of 20–24 ovaries. A circle or ellipse indicates a GCN. Arrowheads indicate healthy germ cells within the nest; arrows indicate degenerating germ cells. The width of field for each image is 220 or 350 μm. EI, eosinophilic infiltration (red staining). $^*P < 0.05$, control vs. CrVI.

facilitate the resorption of apoptotic and/or degenerating germ cells.

The ECM provides structural support to the follicle, maintains cellular organization and connectivity, and provides biochemical signals that promote follicle development and maturation [30]. However, the specific role of ECM in GCN breakdown or early development of the follicles is unknown. *Xpnpep2* is one of the marker genes for POF [18], and it hydrolyzes Cols [27]. The current study shows, to our knowledge for the first time, that *Xpnpep2* is involved in GCN breakdown under normal physiological conditions and that CrVI advances and accelerates GCN breakdown by up-regulating Xpnpep2 and decreasing the distribution of Col1, Col3, and Col4 in the fetal ovary on ED 15.5 and ED 17.5. A negative correlation between the abundance of Cols and Xpnpep2 during ED 15.5 and ED 17.5 suggested that Xpnpep2 may be a direct regulator of Cols during GCN breakdown. To confirm this, we colocalized Xpnpep2 with Col3 and Col4 in the ovarian whole mounts. In both control and CrVI-exposed ovaries, Xpnpep2 was colocalized with Col3 and Col4 along the ovigerous cords, within the GCN, and around the germ cells. CrVI advanced GCN breakdown and increased the penetration of somatic cells within the GCN on ED 15.5. Furthermore, in the control group, GCN breakdown began on ED 17.5 while, at the same time point, GCN breakdown had already reached a maximum in the CrVI group. In both control and CrVI groups, Xpnpep2 colocalization with Col3 and Col4 was stronger on ED 17.5. This suggests that whether under normal physiological conditions or CrVI exposure, Xpnpep2 may regulate hydrolysis of Cols to facilitate GCN breakdown and that CrVI advanced GCN breakdown by up-regulation of Xpnpep2.

We hypothesized that Xpnpep2 may also play critical roles in various stages of follicle development beyond GCN breakdown—namely, during postnatal ovarian development. Therefore, we monitored expression of Xpnpep2 protein in the ovaries of rats at PND 1, PND 4, and PND 25 under normal physiological conditions and following gestational exposure to CrVI. Interestingly, we observed a spatiotemporal pattern of Xpnpep2 expression during primordial follicle assembly and primary follicle transition. In control ovaries, Xpnpep2 expression was elevated from ED 17.5 to PND 1, a peak window for GCN breakdown. Its expression declined on PND 4 and PND 25. Interestingly, on PND 4 and PND 25, Xpnpep2 was predominantly expressed in the oocytes. On the other hand, unlike in the fetal ovaries, CrVI down-regulated Xpnpep2 on PND 1, PND 4, and PND 25, when an increase in follicle atresia was found compared to control. Xpnpep2 is expressed in the ovary during development, and it may function to regulate paracrine signaling [18]. In the CrVI group, a corresponding increase was found in Col1, Col3, and Col4 in the PND 1, PND 4, and PND 25 ovaries, as opposed to the expression of Xpnpep2. These observations suggest that increased Cols may have altered the histoarchitecture of the ovary and microenvironment of the follicles, thus preventing intercellular communication and/or paracrine signaling and thereby follicle growth. Primordial follicle assembly takes

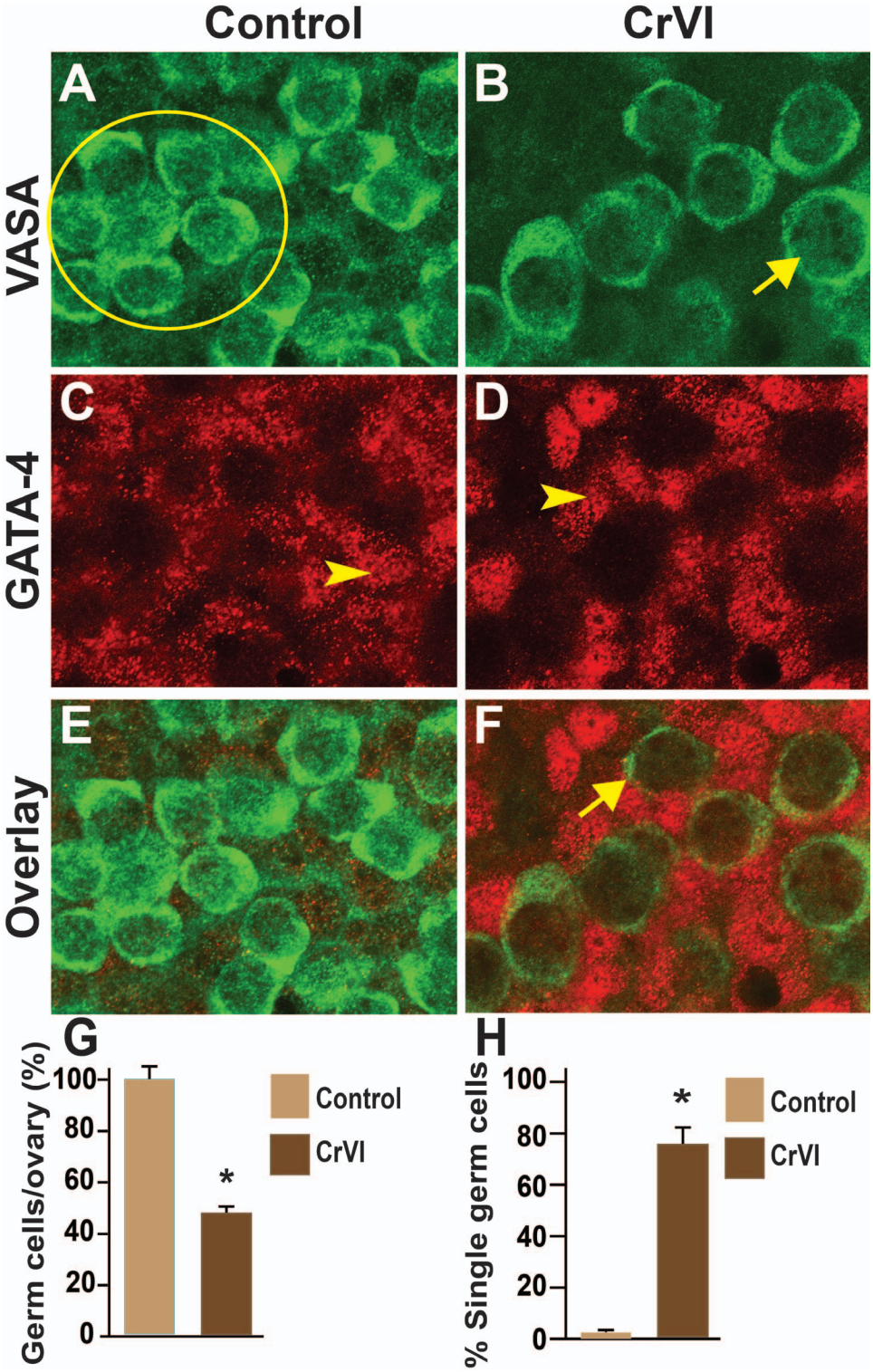

FIG. 4. Effects of prenatal exposure to CrVI on GCN breakdown in the fetal ovary on ED 15.5. Ovaries from ED 15.5 were processed for whole-mount double immunofluorescence assay and imaged by confocal microscopy. Germ cells were identified by Vasa immunostaining (green; **A** and **B**) and somatic cells by Gata4 immunostaining (red; **C** and **D**), with overlays shown (**E** and **F**). The average number of germ cells or oocytes per ovary (**G**) and the percentage of single oocytes (**H**) are also shown. Arrows indicate germ cells; arrowheads indicate somatic cells. A circle or ellipse indicates a GCN. The width of field for each image is 115 μm. *$P < 0.05$, control vs. CrVI.

place in rodents during the early postnatal period. This involves migration of somatic (pregranulosa) cells to surround oocytes. Interestingly, CrVI down-regulated Xpnpep2 during the postnatal period (PNDs 1–4). Inhibition of the hydrolysis of Cols resulted in the accumulation of Cols in the intra- and interfollicular compartments, which may have contributed to the increased atresia of follicles in the CrVI-exposed ovaries. Further investigation is needed to explore and confirm the precise role of Xpnpep2 in various cell signaling pathways that control GCN breakdown, follicle development, and POF.

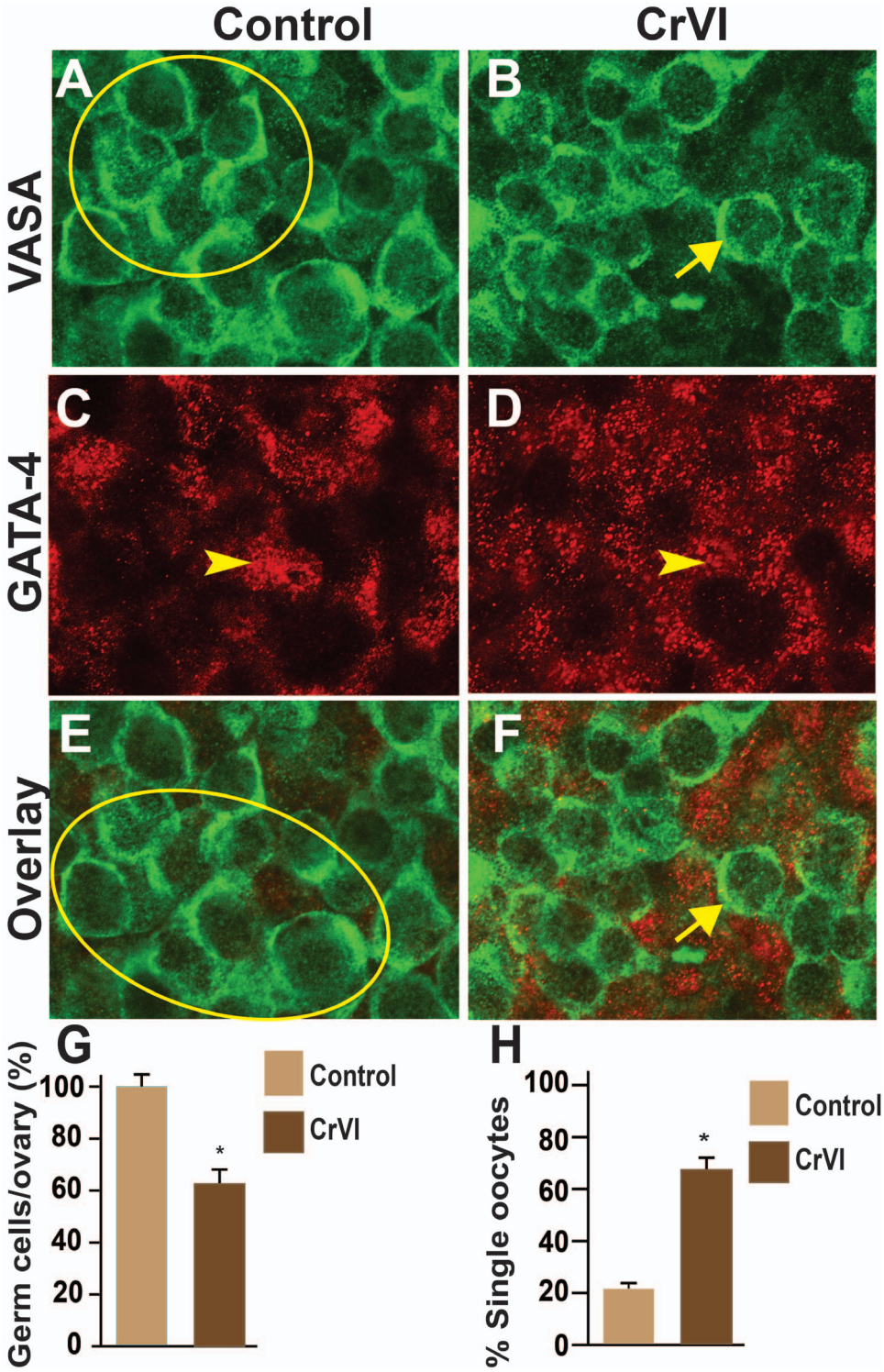

FIG. 5. Effects of prenatal exposure to CrVI on GCN breakdown in the fetal ovary on ED 17.5. Ovaries from ED 17.5 were processed for whole-mount double immunofluorescence assay and imaged by confocal microscopy. Germ cells were identified by Vasa immunostaining (green; **A** and **B**) and somatic cells by Gata4 immunostaining (red; **C** and **D**), with overlays shown (**E** and **F**). The average number of germ cells or oocytes per ovary (**G**) and the percentage of single oocytes (**H**) are also shown. Arrows indicate germ cells; arrowheads indicate somatic cells. A circle or ellipse indicates a GCN. The width of field for each image is 115 μm. *$P < 0.05$, control vs. CrVI.

Numerous studies have indicated the uniqueness of the intrinsic properties of ECM in different niches and tissue-level compartments that can impact cell polarization, proliferation, growth and differentiation, cell survival, and programmed cell death [82–85], including the process of follicle development. In addition to providing a rigid or elastic mechanical support for follicles, nutrients and hormones and other extracellular signals often must traverse the matrix to reach granulosa cells. The follicular basal lamina, which typically forms a continuous layer and associates with granulosa cells in the ovaries, is highly enriched in Col4 [28, 86]. Col1 and Col3 (fibrillar and interstitial) are predominantly in connective tissues, whereas

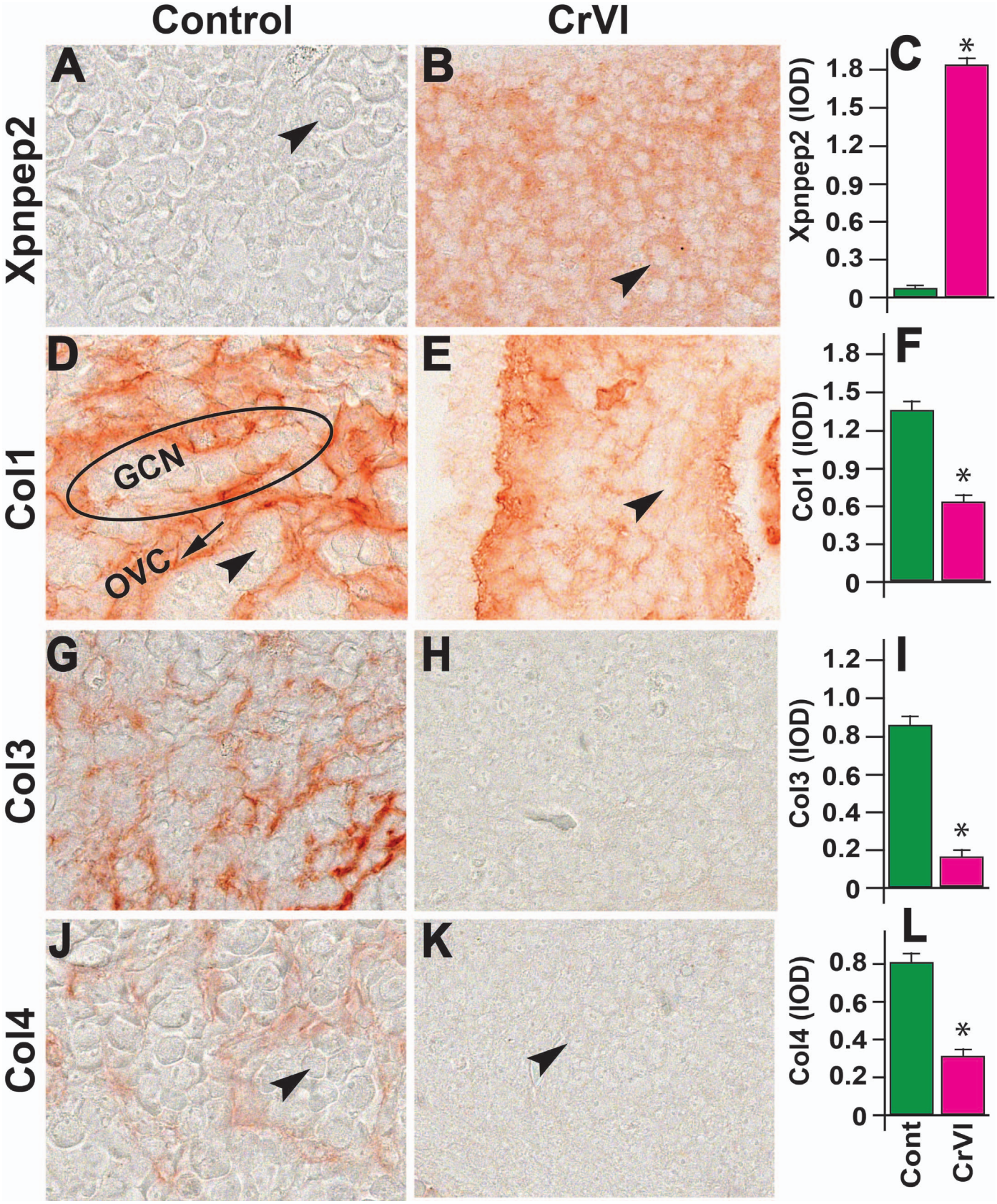

FIG. 6. Effects of prenatal exposure to CrVI on the expression of Xpnpep2 (**A**–**C**), Col1 (**D**–**F**), Col3 (**G**–**I**), and Col4 (**J**–**L**) proteins in the ED 15.5 ovaries. Ovaries from ED 15.5 fetuses were processed for IHC, and the integrated optical density (IOD) of staining was quantified using Image ProPlus software. The width of field for each image is 220 or 350 μm. Arrowheads indicate germ cells. An ellipse indicates a GCN; an arrow indicates ovigerous cord (OVC). Each value represents the mean ± SEM of 20–24 ovaries. *$P < 0.05$, control vs. CrVI.

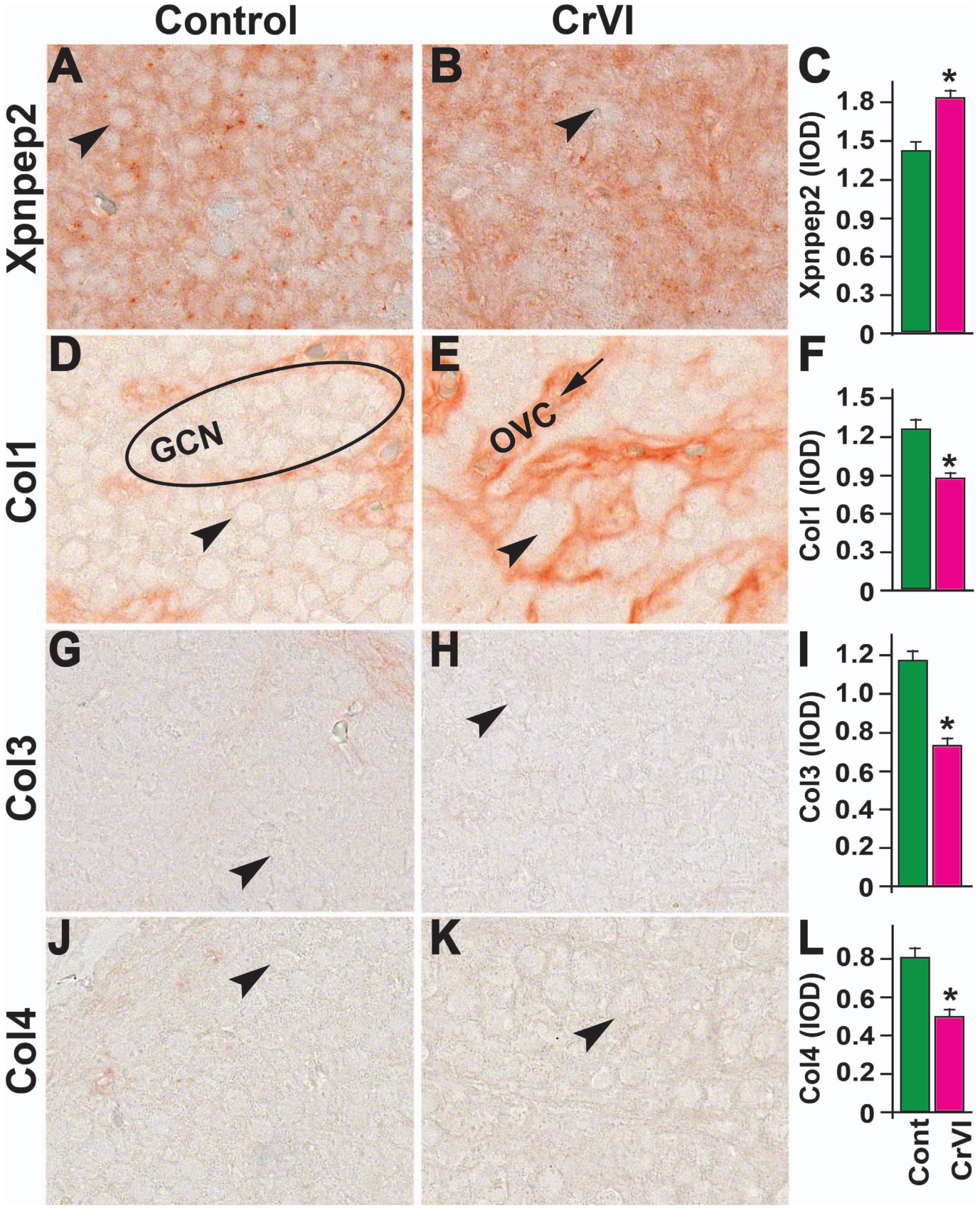

FIG. 7. Effects of prenatal exposure to CrVI on the expression of Xpnpep2 (**A**–**C**), Col1 (**D**–**F**), Col3 (**G**–**I**), and Col4 (**J**–**L**) proteins in the ED 17.5 ovaries. Ovaries from ED 17.5 fetuses were processed for IHC and the integrated optical density (IOD) of staining was quantified using Image ProPlus software. The width of field for each image is 220 or 350 μm. Arrowheads indicate germ cells. An ellipse indicates a GCN; an arrow indicates ovigerous cord (OVC). Each value represents the mean ± SEM of 20–24 ovaries. *$P < 0.05$, control vs. CrVI.

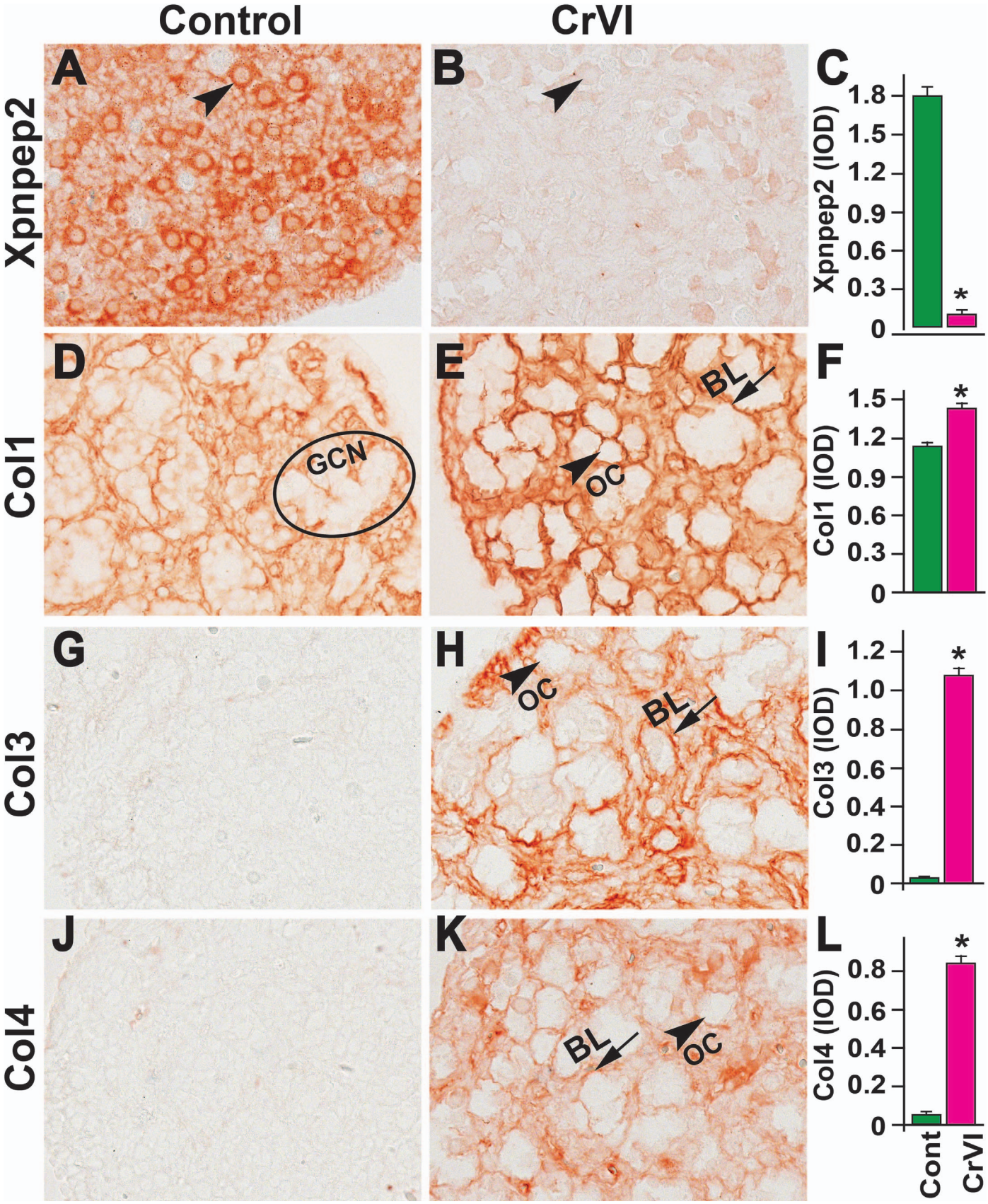

FIG. 8. Effects of prenatal exposure to CrVI on the expression of Xpnpep2 (**A**–**C**), Col1 (**D**–**F**), Col3 (**G**–**I**), and Col4 (**J**–**L**) proteins in the PND 1 ovaries. Ovaries from PND 1 pups (F1) were processed for IHC and the integrated optical density (IOD) of staining was quantified using Image ProPlus software. The width of field for each image is 220 or 350 μm. Arrowheads indicate germ cells or oocytes (OC); arrows indicate ovigerous cord basal lamina (BL) of the follicles. An ellipse indicates a GCN. Each value represents the mean ± SEM of 15–18 ovaries. *$P < 0.05$, control vs. CrVI.

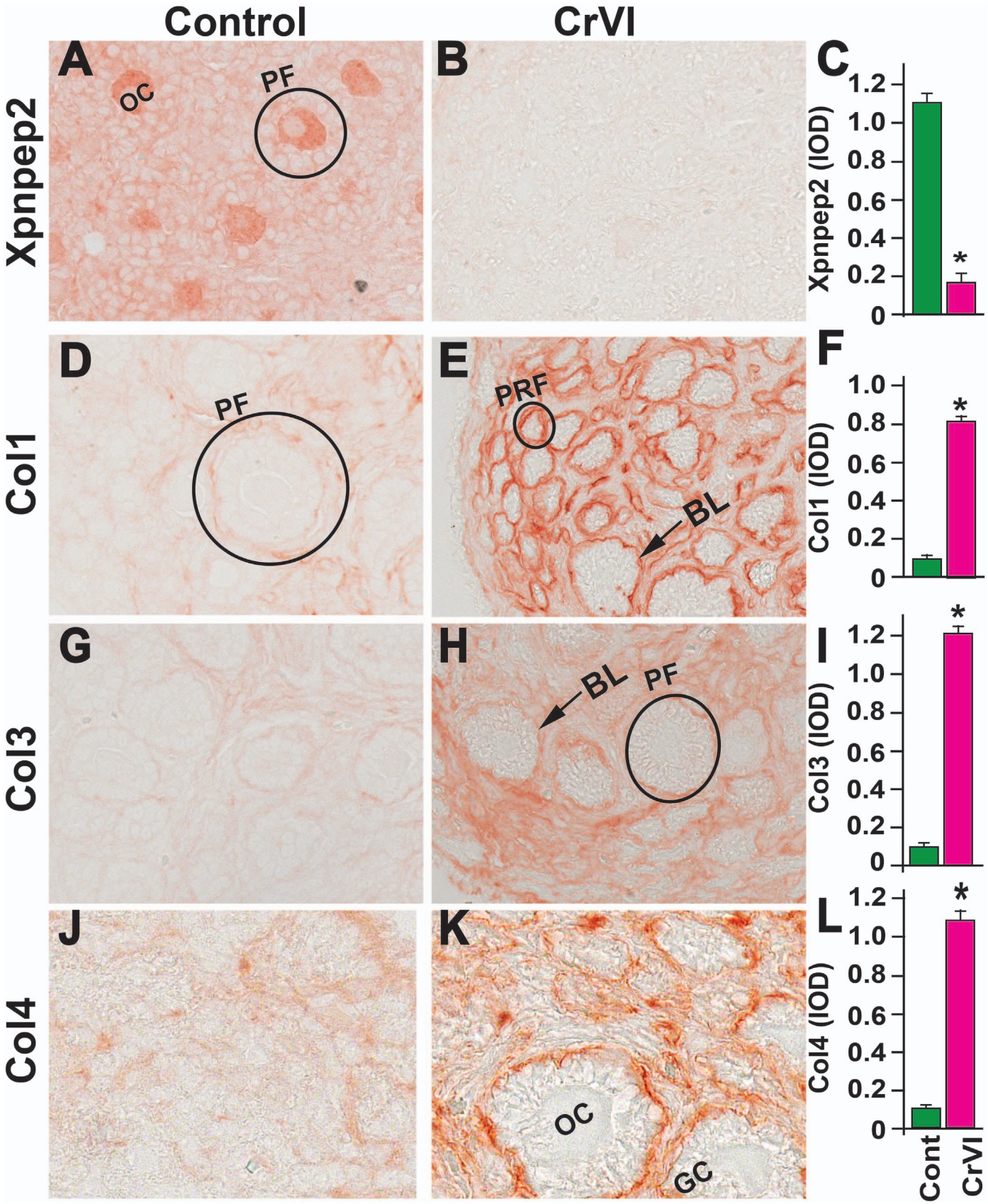

FIG. 9. Effects of prenatal exposure to CrVI on the expression of Xpnpep2 (**A**–**C**), Col1 (**D**–**F**), Col3 (**G**–**I**), and Col4 (**J**–**L**) proteins in the PND 4 ovaries. Ovaries from PND 4 pups (F1) were processed for IHC and the integrated optical density (IOD) of staining was quantified using Image ProPlus software. The width of field for each image is 220 or 350 μm. Each value represents the mean ± SEM of 20–24 ovaries. Arrows indicate basal lamina (BL) of the follicle. A circle or ellipse indicates a primordial follicle (PRM) or primary follicle (PF). OC, oocyte; GC, granulosa cell. *$P < 0.05$, control vs. CrVI.

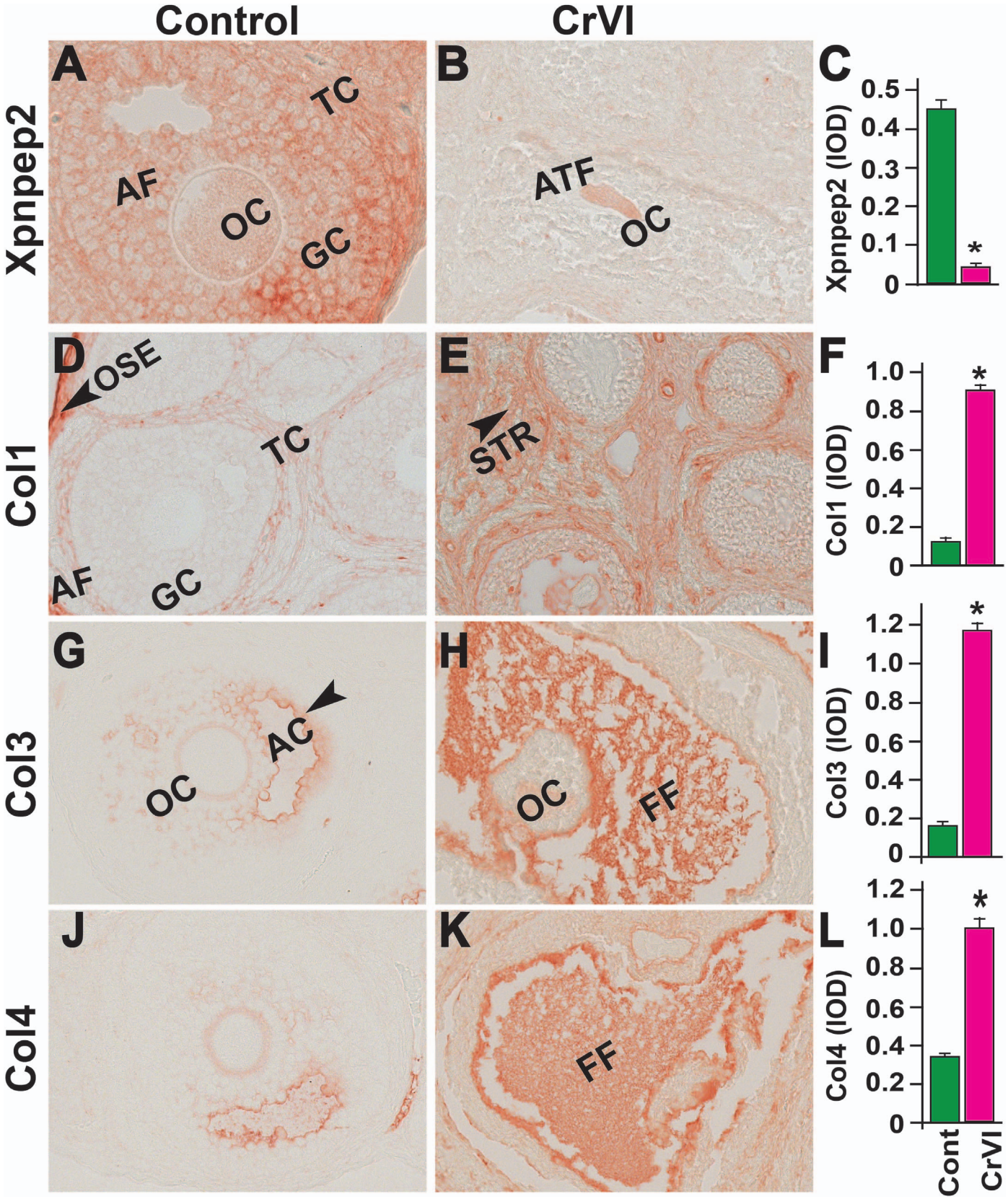

FIG. 10. Effects of prenatal exposure to CrVI on the expression of Xpnpep2 (**A**–**C**), Col1 (**D**–**F**), Col3 (**G**–**I**), and Col4 (**J**–**L**) proteins in the PND 25 ovaries. Ovaries from PND 25 pups (F1) were processed for IHC and the integrated optical density (IOD) of staining was quantified using Image ProPlus software. The width of field for each image is 220 or 350 μm. Each value represents the mean ± SEM of 20–24 ovaries. OC, oocyte; GC, granulosa cells; TC, theca cells; ATF, atretic follicle; STR, stroma; AC, antral cavity; FF, follicular fluid. *$P < 0.05$, control vs. CrVI.

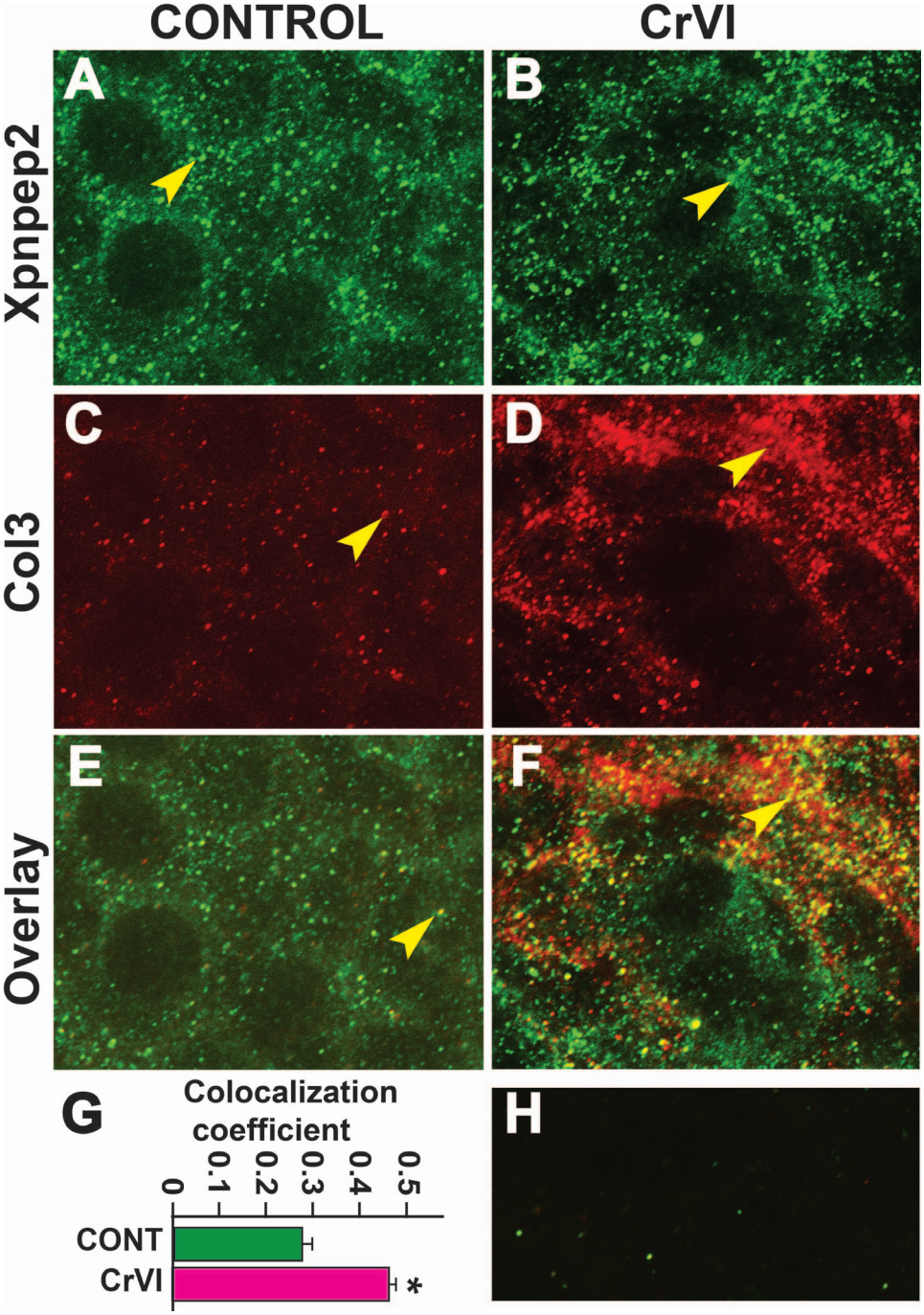

FIG. 11. Effects of prenatal exposure to CrVI on colocalization of Xpnpep2 and Col3 proteins in the ED 17.5 ovaries. On ED 17.5, ovaries from fetuses were processed for whole-mount double immunofluorescence assay. Colocalization of Xpnpep2 and Col3 proteins was evaluated by confocal microscopy. CrVI significantly increased colocalization of Xpnpep2 and Col3 proteins compared to control (overlay; **E** and **F**). Width of the images was 115 μm. Arrowheads indicate localization of Xpnpep2 (**A** and **B**), localization of Col3 (**C** and **D**), and colocalization of Xpnpep2 and Col4 (**E** and **F**) in a GCN. Histogram of colocalization coefficient (**G**), and negative control (**H**) are shown. *$P < 0.05$, control vs. CrVI.

Col4 (network) is exclusively present in the basal lamina [28, 29]. Thus, we also examined the changes in localization and expression levels and pattern of interstitial Col1 and Col3 and basal lamina Col4 during GCN breakdown and early follicle development along with the effects of CrVI on the expression pattern of these Cols. During follicle development, the follicular basal lamina becomes less Col and more laminin rich, providing an expandable basal lamina that is required for follicle development [87]. Both control and CrVI groups had lower levels of Col3 and Col4 on ED 17.5, a time point when GCN breakdown commenced in the control group and reached a peak in the CrVI group. It is suggested that degradation or hydrolysis of Col3 and Col4 may facilitate GCN breakdown. Interestingly, on PND 1 and PND 4, CrVI up-regulated both Col3 and Col4, whereas Col3 and Col4 were barely detectable in controls. Many ECM proteins have binding sites for growth factors. The ECM also sequesters and provides a repository for cytokines, enzymes, and growth factors [88]. Degradation of ECM components liberates these active molecules. CrVI increased folding of the basal lamina and accumulation of

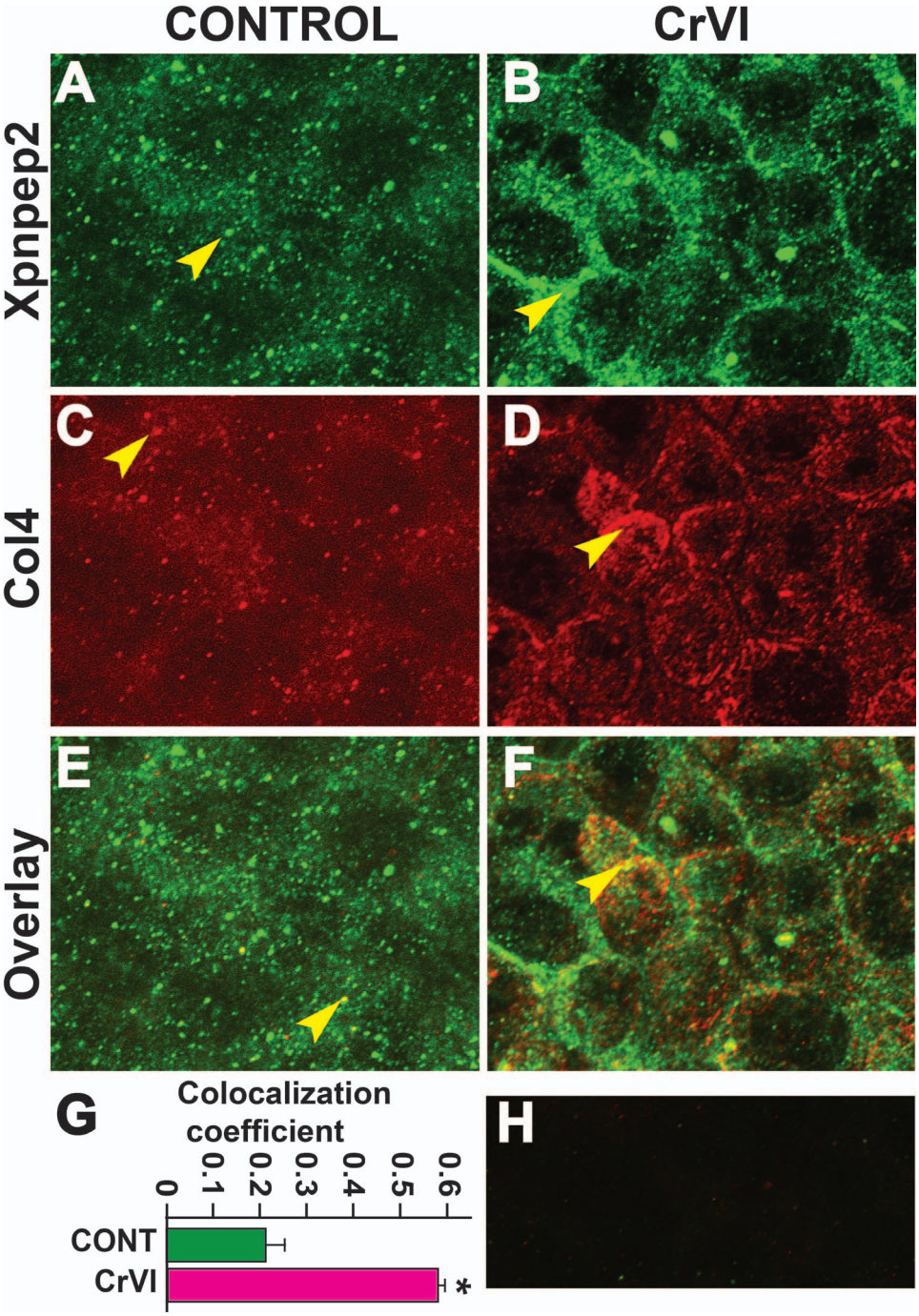

FIG. 12. Effects of prenatal exposure to CrVI on colocalization of Xpnpep2 and Col4 proteins in the ED 17.5 ovaries. On ED 17.5, ovaries from fetuses were processed for whole-mount double immunofluorescence assay. Colocalization of Xpnpep2 and Col4 proteins was evaluated by confocal microscopy. CrVI significantly increased colocalization of Xpnpep2 and Col4 proteins compared to control (overlay; **E** and **F**). The width of field for images was 115 μm. Arrowheads indicate localization of Xpnpep2 (**A** and **B**), localization of Col4 (**C** and **D**), and colocalization of Xpnpep2 and Col4 (**E** and **F**) in a GCN. Histogram of colocalization coefficient (**G**) and negative control (**H**) are shown. *$P < 0.05$, control vs. CrVI.

Col in the follicular compartment. It is possible that increased accumulation of Col may have inhibited the distribution of active growth factors required for follicle development and survival.

Taken together, the current results suggest that 1) Xpnpep2 may play a critical role during GCN breakdown and primordial follicle assembly by regulating the distribution of Cols during normal development of the ovary, 2) CrVI up-regulates Xpnpep2 and decreases Col distribution in a spatiotemporal pattern during GCN breakdown, 3) CrVI down-regulates Xpnpep2 and up-regulates Col during primordial follicle assembly, and 4) CrVI induces decreased expression of Xpnpep2 and increased accumulation of Cols that eventually leads to an increase in follicle atresia. These novel findings suggest, to our knowledge for the first time, that disruption of the *Xpnpep2* gene in women with POF may result in abnormal accumulation of Cols, follicle atresia, and early reproductive senescence or infertility. Xpnpep2 could also be a target for heavy metal EDCs that impact follicle development by altering the ratio of Cols.

ACKNOWLEDGMENT

Confocal microscopy was performed in the Texas A&M University College of Veterinary Medicine & Biomedical Sciences Image Analysis Laboratory.

REFERENCES

1. Nippita TA, Baber RJ. Premature ovarian failure: a review. Climacteric 2007; 10:11–22.
2. Cox L, Liu JH. Primary ovarian insufficiency: an update. Int J Womens Health 2014; 6:235–243.
3. Sivakumar KK, Stanley JA, Arosh JA, Pepling ME, Burghardt RC, Banu SK. Prenatal exposure to chromium induces early reproductive senescence by increasing germ cell apoptosis and advancing germ cell cyst breakdown in the F1 offspring. Dev Biol 2014; 388:22–34.
4. Coulam CB, Adamson SC, Annegers JF. Incidence of premature ovarian failure. Obstet Gynecol 1986; 67:604–606.
5. Cordts EB, Christofolini DM, Dos Santos AA, Bianco B, Barbosa CP. Genetic aspects of premature ovarian failure: a literature review. Arch Gynecol Obstet 2011; 283:635–643.
6. Harris SE, Chand AL, Winship IM, Gersak K, Aittomaki K, Shelling AN. Identification of novel mutations in *FOXL2* associated with premature ovarian failure. Mol Hum Reprod 2002; 8:729–733.
7. Shah D, Nagarajan N. Premature menopause—meeting the needs. Post Reprod Health 2014; 20:62–68.
8. Rivera OE, Varayoud J, Rodríguez HA, Muñoz-de-Toro M, Luque EH. Neonatal exposure to bisphenol A or diethylstilbestrol alters the ovarian follicular dynamics in the lamb. Reprod Toxicol 2011; 32:304–312.
9. Manikkam M, Haque MM, Guerrero-Bosagna C, Nilsson EE, Skinner MK. Pesticide methoxychlor promotes the epigenetic transgenerational inheritance of adult-onset disease through the female germline. PLOS ONE 2014; 9:e102091.
10. Rodríguez HA, Santambrosio N, Santamaría CG, Muñoz-de-Toro M, Luque EH. Neonatal exposure to bisphenol A reduces the pool of primordial follicles in the rat ovary. Reprod Toxicol 2010; 30:550–557.
11. Nilsson E, Larsen G, Manikkam M, Guerrero-Bosagna C, Savenkova MI, Skinner MK. Environmentally induced epigenetic transgenerational inheritance of ovarian disease. PLOS ONE 2012; 7:e36129.
12. Pepling ME. From primordial germ cell to primordial follicle: mammalian female germ cell development. Genesis 2006; 44:622–632.
13. Pepling ME, Spradling AC. Female mouse germ cells form synchronously dividing cysts. Development 1998; 125:3323–3328.
14. Rizzolio F, Sala C, Alboresi S, Bione S, Gilli S, Goegan M, Pramparo T, Zuffardi O, Toniolo D. Epigenetic control of the critical region for premature ovarian failure on autosomal genes translocated to the X chromosome: a hypothesis. Hum Genet 2007; 121:441–450.
15. Therman E, Laxova R, Susman B. The critical region on the human Xq. Hum Genet 1990; 85:455–461.
16. Rizzolio F, Pramparo T, Sala C, Zuffardi O, De Santis L, Rabellotti E, Calzi F, Fusi F, Bellazzi R, Toniolo D. Epigenetic analysis of the critical region I for premature ovarian failure: demonstration of a highly heterochromatic domain on the long arm of the mammalian X chromosome. J Med Genet 2009; 46:585–592.
17. Schlessinger D, Herrera L, Crisponi L, Mumm S, Percesepe A, Pellegrini M, Pilia G, Forabosco A. Genes and translocations involved in POF. Am J Med Genet 2002; 111:328–333.
18. Prueitt RL, Ross JL, Zinn AR. Physical mapping of nine Xq translocation breakpoints and identification of XPNPEP2 as a premature ovarian failure candidate gene. Cytogenet Cell Genet 2000; 89:44–50.
19. Bione S, Rizzolio F, Sala C, Ricotti R, Goegan M, Manzini M, Battaglia R, Marozzi A, Vegetti W, Dalpra L. Mutation analysis of two candidate genes for premature ovarian failure, *DACH2* and *POF1B*. Hum Reprod 2004; 19:2759–2766.
20. Van Bokhoven H, van den Hurk JA, Bogerd L, Philippe C, Gilgenkrantz S, de Jong P, Ropers H-H, Cremers FP. Cloning and characterization of the human choroideremia gene. Hum Mol Genet 1994; 3:1041–1046.
21. Bione S, Sala C, Manzini C, Arrigo G, Zuffardi O, Banfi S, Borsani G, Jonveaux P, Philippe C, Zuccotti M. A human homologue of the *Drosophila melanogaster diaphanous* gene is disrupted in a patient with premature ovarian failure: evidence for conserved function in oogenesis and implications for human sterility. Am J Hum Genet 1998; 62:533–541.
22. Prueitt R, Chen H, Barnes R, Zinn A. Most X;autosome translocations associated with premature ovarian failure do not interrupt X-linked genes. Cytogenet Genome Res 2002; 97:32–38.
23. Venema RC, Ju H, Zou R, Venema VJ, Ryan JW. Cloning and tissue distribution of human membrane-bound aminopeptidase P. Biochim Biophys Acta 1997; 1354:45–48.
24. Sprinkle TJ, Stone AA, Venema RC, Denslow ND, Caldwell C, Ryan JW. Assignment of the membrane-bound human aminopeptidase P gene (XPNPEP2) to chromosome Xq25. Genomics 1998; 50:114–116.
25. Molinaro G, Boileau G, Adam A. Aminopeptidase P and vasoactive peptides. In: Hooper N, Lendeckel U (eds.), Aminopeptidases in Biology and Disease, vol. 2. New York: Springer; 2004:251–269.
26. Fietzek PP, Kühn K. The primary structure of collagen. Int Rev Connect Tissue Res 1976; 7:1–60.
27. McDonald JK, Hoisington AR, Eisenhauer DA. Partial purification and characterization of an ovarian tripeptidyl peptidase: a lysosomal exopeptidase that sequentially releases collagen-related (Gly-Pro-X) triplets. Biochem Biophys Res Commun 1985; 126:63–71.
28. Nakano K, Naito I, Momota R, Sado Y, Hasegawa H, Ninomiya Y, Ohtsuka A. The distribution of type IV collagen alpha chains in the mouse ovary and its correlation with follicular development. Arch Histol Cytol 2007; 70:243–253.
29. Berkholtz CB, Lai BE, Woodruff TK, Shea LD. Distribution of extracellular matrix proteins type I collagen, type IV collagen, fibronectin, and laminin in mouse folliculogenesis. Histochem Cell Biol 2006; 126: 583–592.
30. Rodgers R, Van Wezel I, Irving-Rodgers H, Lavranos T, Irvine C, Krupa M. Roles of extracellular matrix in follicular development. J Reprod Fertil Suppl 1999; 54:343–352.
31. Aharoni D, Meiri I, Atzmon R, Vlodavsky I, Amsterdam A. Differential effect of components of the extracellular matrix on differentiation and apoptosis. Curr Biol 1997; 7:43–51.
32. Oktay K, Karlikaya G, Akman O, Ojakian GK, Oktay M. Interaction of extracellular matrix and activin-A in the initiation of follicle growth in the mouse ovary. Biol Reprod 2000; 63:457–461.
33. Rodgers RJ, Irving-Rodgers HF. Extracellular matrix of the bovine ovarian membrana granulosa. Mol Cell Endocrinol 2002; 191:57–64.
34. Irving-Rodgers HF, Rodgers RJ. Extracellular matrix of the developing ovarian follicle. Semin Reprod Med 2006; 24:195–203.
35. Irving-Rodgers HF, Catanzariti KD, Aspden WJ, D'Occhio MJ, Rodgers RJ. Remodeling of extracellular matrix at ovulation of the bovine ovarian follicle. Mol Reprod Dev 2006; 73:1292–1302.
36. Bagavandoss P. Temporal expression of tenascin-C and type I collagen in response to gonadotropins in the immature rat ovary. Acta Histochem 2014; 116:1125–1133.
37. Woodruff TK, Shea LD. The role of the extracellular matrix in ovarian follicle development. Reprod Sci 2007; 14:6–10.
38. Zalewski A, Cecchini EL, Deroo BJ. Expression of extracellular matrix components is disrupted in the immature and adult estrogen receptor β-null mouse ovary. PLOS ONE 2012; 7:e29937.
39. Banu SK. Heavy metals and the ovary. In: Hoyer PB (ed.), Ovarian Toxicology, 2nd ed. Boca Raton, FL: CRC Press; 2013:191–228.
40. Shanker AK, Venkateswarlu B. Chromium: Environmental Pollution, Health Effects and Mode of Action. In: Nriagu JO (ed.), Encyclopedia of Environmental Health. Burlington, VT: Elsevier; 2011:650–659.
41. Pellerin C, Booker SM. Reflections on hexavalent chromium: health hazards of an industrial heavyweight. Environ Health Perspect 2000; 108: A402–A407.
42. Sutton R. Chromium-6 in U.S. Tap Water. Washington, DC: Environmental Working Group; 2010.
43. Shmitova LA. Content of hexavalent chromium in the biological substrates of pregnant women and puerperae engaged in the manufacture of chromium compounds [in Russian]. Gig Tr Prof Zabol 1980; Feb:33–35.
44. Jendryczko A, Drozdz M, Magner K. Preliminary studies of chromium concentration in the myometrium in the third trimester of pregnancy, in chorionic tissue in the first trimester and in the blood of pregnant women [in Polish]. Ginekol Pol 1984; 55:691–694.
45. Greene LE, Riederer AM, Marcus M, Lkhasuren O. Associations of fertility and pregnancy outcomes with leather tannery work in Mongolia: a pilot study. Int J Occup Environ Health 2010; 16:60–68.
46. Zhang J, Cai WW, Lee DJ. Occupational hazards and pregnancy outcomes. Am J Ind Med 1992; 21:397–408.
47. Quansah R, Jaakkola JJ. Paternal and maternal exposure to welding fumes and metal dusts or fumes and adverse pregnancy outcomes. Int Arch Occup Environ Health 2009; 82:529–537.
48. Hemminki K, Kyyronen P, Niemi ML, Koskinen K, Sallmen M, Vainio H. Spontaneous abortions in an industrialized community in Finland. Am J Public Health 1983; 73:32–37.
49. Hemminki K, Niemi ML, Koskinen K, Vainio H. Spontaneous abortions among women employed in the metal industry in Finland. Int Arch Occup Environ Health 1980; 47:53–60.

50. Yang Y, Liu H, Xiang XH, Liu FY. Outline of occupational chromium poisoning in China. Bull Environ Contam Toxicol 2013; 90:742–749.
51. Flora SJS, Pachauri V, Saxena G. Arsenic, cadmium and lead. In: Gupta RC (ed.), Reproductive and Developmental Toxicity. San Diego; Academic Press; 2011:415–438.
52. Stanley JA, Sivakumar KK, Arosh JA, Burghardt RC, Banu SK. Edaravone mitigates hexavalent chromium-induced oxidative stress and depletion of antioxidant enzymes while estrogen restores antioxidant enzymes in the rat ovary in F1 offspring. Biol Reprod 2014; 91:12.
53. Stanley JA, Sivakumar KK, Nithy TK, Arosh JA, Hoyer PB, Burghardt RC, Banu SK. Postnatal exposure to chromium through mother's milk accelerates follicular atresia in F1 offspring through increased oxidative stress and depletion of antioxidant enzymes. Free Radic Biol Med 2013; 61C:179–196.
54. Bagchi D, Bagchi M, Stohs S. Chromium (VI)-induced oxidative stress, apoptotic cell death and modulation of p53 tumor suppressor gene. In: Shi X, Castranova V, Vallyathan V, Perry W (eds.), Molecular Mechanisms of Metal Toxicity and Carcinogenesis, vol. 34. New York: Springer; 2001:149–158.
55. Zhitkovich A. Importance of chromium-DNA adducts in mutagenicity and toxicity of chromium(VI). Chem Res Toxicol 2005; 18:3–11.
56. Balachandar V, Arun M, Devi SM, Velmurugan P, Manikantan P, Kumar AK, Sasikala K, Venkatesan C. Evaluation of the genetic alterations in direct and indirect exposures of hexavalent chromium [Cr(VI)] in leather tanning industry workers North Arcot District, South India. Int Arch Occup Environ Health 2010; 83:791–801.
57. Figgitt M, Newson R, Leslie IJ, Fisher J, Ingham E, Case CP. The genotoxicity of physiological concentrations of chromium (Cr(III) and Cr(VI)) and cobalt (Co(II)): an in vitro study. Mutat Res 2010; 688:53–61.
58. Velma V, Tchounwou PB. Chromium-induced biochemical, genotoxic and histopathologic effects in liver and kidney of goldfish, *Carassius auratus*. Mutat Res 2010; 698:43–51.
59. Arita A, Costa M. Epigenetics in metal carcinogenesis: nickel, arsenic, chromium and cadmium. Metallomics 2009; 1:222–228.
60. Devine PJ, Perreault SD, Luderer U. Roles of reactive oxygen species and antioxidants in ovarian toxicity. Biol Reprod 2012; 86:21–10.
61. Kim JK, Lee CJ. Effect of exogenous melatonin on the ovarian follicles in γ-irradiated mouse. Mutat Res 2000; 449:33–39.
62. Hashiguchi K, Stuart J, de Souza-Pinto N, Bohr V. The C-terminal αO helix of human Ogg1 is essential for 8-oxoguanine DNA glycosylase activity: the mitochondrial β-Ogg1 lacks this domain and does not have glycosylase activity. Nucleic Acids Res 2004; 32:5596–5608.
63. Yamane A, Kohno T, Ito K, Sunaga N, Aoki K, Yoshimura K, Murakami H, Nojima Y, Yokota J. Differential ability of polymorphic OGG1 proteins to suppress mutagenesis induced by 8-hydroxyguanine in human cell in vivo. Carcinogenesis 2004; 25:1689–1694.
64. Vidal AE, Boiteux S, Hickson ID, Radicella JP. XRCC1 coordinates the initial and late stages of DNA abasic site repair through protein–protein interactions. EMBO J 2001; 20:6530–6539.
65. Hu YC, Ahrendt SA. *hOGG1* Ser326Cys polymorphism and G:C-to-T:A mutations: no evidence for a role in tobacco-related non small cell lung cancer. Int J Cancer 2005; 114:387–393.
66. Baccarelli A, Bollati V. Epigenetics and environmental chemicals. Curr Opin Pediatr 2009; 21:243–251.
67. Martinez-Zamudio R, Ha HC. Environmental epigenetics in metal exposure. Epigenetics 2011; 6:820–827.
68. Mishra S, Dwivedi SP, Singh R. A review on epigenetic effect of heavy metal carcinogens on human health. Open Nutraceuticals J 2010; 3: 188–193.
69. Xia B, Ren X-h, Zhuang Z-x, Yang L-q, Huang H-y, Pang L, Wu D-s, Luo J, Tan Y-l, Liu J-j. Effect of hexavalent chromium on histone biotinylation in human bronchial epithelial cells. Toxicol Lett 2014; 228:241–247.
70. Labra M, Grassi F, Imazio S, Di Fabio T, Citterio S, Sgorbati S, Agradi E. Genetic and DNA-methylation changes induced by potassium dichromate in *Brassica napus* L. Chemosphere 2004; 54:1049–1058.
71. Kondo K, Takahashi Y, Hirose Y, Nagao T, Tsuyuguchi M, Hashimoto M, Ochiai A, Monden Y, Tangoku A. The reduced expression and aberrant methylation of $p16^{INK4a}$ in chromate workers with lung cancer. Lung Cancer 2006; 53:295–302.
72. Devine PJ, Sipes IG, Skinner MK, Hoyer PB. Characterization of a rat in vitro ovarian culture system to study the ovarian toxicant 4-vinylcyclohexene diepoxide. Toxicol Appl Pharmacol 2002; 184:107–115.
73. Lee J, Banu SK, Nithy TK, Stanley JA, Arosh JA. Early pregnancy induced expression of prostaglandin E2 receptors EP2 and EP4 in the ovine endometrium and regulated by interferon tau through multiple cell signaling pathways. Mol Cell Endocrinol 2012; 348:211–223.
74. Pepling ME, Spradling AC. Mouse ovarian germ cell cysts undergo programmed breakdown to form primordial follicles. Dev Biol 2001; 234: 339–351.
75. Takagi K, Yamada T, Miki Y, Umegaki T, Nishimura M, Sasaki J. Histological observation of the development of follicles and follicular atresia in immature rat ovaries. Acta Med Okayama 2007; 61:283–298.
76. Hirshfield AN. Development of follicles in the mammalian ovary. Int Rev Cytol 1991; 124:43–101.
77. Hirshfield AN. Overview of ovarian follicular development: considerations for the toxicologist. Environ Mol Mutagen 1997; 29:10–15.
78. Hirshfield AN, DeSanti AM. Patterns of ovarian cell proliferation in rats during the embryonic period and the first three weeks postpartum. Biol Reprod 1995; 53:1208–1221.
79. Hirshfield AN. Relationship between the supply of primordial follicles and the onset of follicular growth in rats. Biol Reprod 1994; 50:421–428.
80. Gleich GJ, Loegering DA, Bell MP, Checkel JL, Ackerman SJ, McKean DJ. Biochemical and functional similarities between human eosinophil-derived neurotoxin and eosinophil cationic protein: homology with ribonuclease. Proc Natl Acad Sci U S A 1986; 83:3146–3150.
81. Nathan CF, Klebanoff SJ. Augmentation of spontaneous macrophage-mediated cytolysis by eosinophil peroxidase. J Exp Med 1982; 155: 1291–1308.
82. Meredith JE Jr, Fazeli B, Schwartz MA. The extracellular matrix as a cell survival factor. Mol Biol Cell 1993; 4:953–961.
83. Shi YB, Li Q, Damjanovski S, Amano T, Ishizuya-Oka A. Regulation of apoptosis during development: input from the extracellular matrix (review). Int J Mol Med 1998; 2:273–282.
84. Gerard C, Goldbeter A. The balance between cell cycle arrest and cell proliferation: control by the extracellular matrix and by contact inhibition. Interface Focus 2014; 4:20130075.
85. Hubmacher D, Apte SS. The biology of the extracellular matrix: novel insights. Curr Opin Rheumatol 2013; 25:65–70.
86. Kato Y, Ogiwara K, Fujimori C, Kimura A, Takahashi T. Expression and localization of collagen type IV alpha1 chain in medaka ovary. Cell Tissue Res 2010; 340:595–605.
87. Rodgers RJ, Irving-Rodgers HF, Russell DL. Extracellular matrix of the developing ovarian follicle. Reproduction 2003; 126:415–424.
88. Macri L, Silverstein D, Clark RA. Growth factor binding to the pericellular matrix and its importance in tissue engineering. Adv Drug Deliv Rev 2007; 59:1366–1381.